

Double layer in ionic liquids: capacitance vs. temperature from atomistic simulations

Heigo Ers^a, Iuliia V. Voroshylova^b, Piret Pikma^a, Vladislav B. Ivaništšev^{a,c*}

^a Institute of Chemistry, University of Tartu, Ravila 14a, Tartu 50411, Estonia

^b LAQV@REQUIMTE, Faculdade de Ciências, Universidade do Porto, Departamento de Química e Bioquímica, Rua do Campo Alegre, 4169-007 Porto, Portugal

^c Department of Chemistry, Center for High Entropy Alloy Catalysis, University of Copenhagen (UCPH), 2100 Copenhagen Ø, Denmark

Corresponding author email: vliv@chem.ku.dk

Keywords: graphene, differential capacitance, temperature dependence, interfacial structure, molecular dynamics, electrical double layer, 1-ethyl-3-methylimidazolium tetrafluoroborate

Abstract

In this study, we investigated the graphene–ionic liquid (EMImBF₄) interface to clarify the effects of ambient temperature and potential on the differential capacitance. We complemented molecular dynamics simulations with density functional theory calculations to unravel the electrolyte and electrode contributions to the differential capacitance. As a result, we show: (1) the relation of characteristic saddle points of the capacitance–potential curve to the structural changes; (2) the smearing effect of temperature on the local structure and, consequently, on the capacitance; (3) rationalization of these observations with the interfacial bilayer model; and, finally, (4) how quantum capacitance correction dampens the influence of temperature and improves the agreement with the experimental data. These insights are of fundamental and practical importance for the application of similar interfaces in electrochemical energy storage and transformation devices, such as capacitors and actuators.

1. Introduction

Ionic liquids (ILs) are solvent-free electrolytes with exceptional properties. They are characterized by high electrochemical stability and low vapor pressure, making them attractive for use in fuel cells, solar panels, supercapacitors, and electric actuators [1–6]. The interfacial properties of ILs are also of fundamental interest, as their electrical double layer (EDL) differs significantly from the one formed in aqueous and organic electrolytes. That is due to the high concentration of ions, which leads to the layered IL structure and overscreening phenomenon [7,8]. For these reasons, the EDL in IL is actively studied theoretically [9–13], experimentally [14–17], as well as using computational chemistry methods such as molecular dynamics (MD) [18–23] and density functional theory (DFT) [24–26] with increasingly complex models [27–29]. Despite numerous studies, multiple open questions about ILs interfacial properties remain. One of such questions is the nature of differential capacitance (C) dependence on temperature (T).

The T -dependence of the EDL properties of ILs was previously studied both experimentally and computationally. Evaluating C is of great interest here because it allows one to compare the derivative of dC/dT from experimental and computational studies. The existing argumentations support both negative and positive dC/dT derivatives. The negative one is consistent with the mean-field theory, while the positive one (“anomalous”) is revealed in theory when accounting for the ion-ion correlation [30–32]. Several experimental works [33–37] investigating the interfaces of ILs consisting of BF_4^- , PF_6^- , TfI^- or TFSI^- anion and imidazolium (Im) or pyridinium (Pyr) ion-based cation with alkyl chains (M = methyl, E = ethyl, P = propyl, B = butyl), mostly with gold, platinum, or glassy carbon electrodes, showed that the increase in T causes an increase in capacitance ($dC/dT > 0$). Silva *et al.* [34], Siinor *et al.* [33], and Lockett *et al.* [37] justified $dC/dT > 0$ by the thermal dissociation of ion associates, which allows ions to compensate for the charge of the electrode more effectively and thereby reduce the width of the charge layer in the electrolyte. Ivaništšev *et al.* [35] associated $dC/dT > 0$ with the mixing of ion layers when increasing T .

In contrast to the studies mentioned above, Drüschel *et al.* [38] showed that the capacitance decreases with increasing T ($dC/dT < 0$) in an experimental study of the gold–BMPyrFAP interface. They associated the effect with two capacitive processes with different T -dependent relaxation times. Several computational works also revealed $dC/dT < 0$. Vatamanu *et al.* [39] studied the interface between PMPyrFSI and graphite with MD simulations. They reasoned $dC/dT < 0$ with the diminishing of the ordered layered structure due to the T increase, which lowers the charge separation in the electrolyte. In the case of rough electrode surfaces, they also pointed out that ions can be in the surface cavities at low T . As the T increases, the placement of ions in the cavities is hindered due to thermal motion, which increases the separation of the electrode and ions (d) and thus reduces the capacitance (assuming $C \sim d^{-1}$). Chen *et al.* [40] observed in MD simulations the $C(T)$ dependence only in the vicinity of the potential of zero charge (PZC). Liu *et al.* [41] showed in MD simulations of the graphite–BMImPF₆ interface that in general $dC/dT < 0$, yet in a narrow potential (U) range, capacitance increases. They associated $dC/dT < 0$ with the attenuation of BMIm⁺ cation adsorption on the graphite surface, allowing the anions to screen the surface charge more effectively. With classical DFT simulations, Shen *et al.* [42] also demonstrated that the effect of T on $C(U)$ is U -dependent and can switch from negative to positive. The $dC/dT > 0$ was also assumed by Kislenko *et al.* [43] by evaluating potential drops in MD simulations of the graphite–BMImPF₆ interface. To conclude, the understanding of the dependence and its underlying causes remains unclear, as different experimental and computational studies described both negative and positive dC/dT dependences within the studied U ranges.

In this work, we modeled the interface between 1-ethyl-3-methylimidazolium tetrafluoroborate (EMImBF₄) and graphene (Gr) using MD and DFT. We focused on the capacitance and structure dependence on the potential and temperature. The MD simulations allowed us to characterize the changes in the structure of the IL near the Gr surface, while the DFT calculations accounted for the semimetallic nature of Gr.

2. Methods

2.1. The studied model and computational method

To simulate the interface between Gr and EMImBF₄ at different T and U values, a model consisting of two rigid Gr sheets with electrodes spaced 9.5 nm apart was constructed. Each Gr sheet consisted of 336 carbon atoms and had an area of 2.98×2.95 nm². The space between the electrodes was filled with 288 EMIm⁺ and 288 BF₄⁻ ions, shown in Fig. 1a, using the Packmol software package [44]. The ions represented an IL with a density close to the experimental data [45].

MD simulations with the constructed model were run stepwise. First, energy minimization was performed using the gradient descent method while maintaining T at 450 K. The energy minimization was followed by two equilibration steps with durations of 0.1 ns (time step 0.5 fs) and 1 ns (time step 1.0 fs), both at 450 K. Followingly, the system was then annealed at 1000, 900, or 800 K for 0.5 ns with a time step of 2.0 fs. Next, to represent the charging of the electrodes with opposite but equal charges, an electric field (E) was applied to the systems in a direction perpendicular to the Gr electrode surface. The E values corresponded to the surface charge density (σ) in the range |0–70| $\mu\text{C}/\text{cm}^2$ and were calculated as $E = \sigma / (\epsilon\epsilon_0)$ using the value of 1.6 as relative permittivity (ϵ). After that, the system was cooled down to the T of 300, 350, 400, or 450 K. The charging and cooling steps both lasted 10 ns (timestep 1.0 fs). As a result, three replicas were obtained for each given E and T . As a final step, to collect the data for further analysis, an additional simulation of 10 ns (1.0 fs timestep) was performed with each of the obtained systems, using a pre-set T and E , defined in previous steps. Snapshots of the simulations were stored every 10 ps.

The NaRIBaS framework was used to prepare each described simulation step [46]. All MD simulations were conducted on the Rocket cluster of HPC Center of the University of Tartu [47] using Gromacs versions 5.1.4 and 2019.5 [48,49]. Simulations were performed in an NVT ensemble using the OPLS-AA force field developed by Lopes *et al.* [50], periodic boundary conditions in directions parallel to the surface plane, and a velocity rescale thermostat [51].

In addition, to estimate the density of states (DOS) for an isolated Gr sheet, DFT calculations were performed using the GPAW 21.6.0 software [52,53]. The calculations were performed using the plane-wave method with a cutoff of 800 eV, Perdew–Burke–Ernzerhof (PBE) exchange-correlation functional [54], and a Gr sheet, consisting of 8 carbon atoms and having an area of 0.21 nm², generated using the ASE Python library [55]. For the Brillouin zone sampling, a 40×40×1 Monkhorst–Pack *k*-point grid was used [56]. The periodic boundary conditions were applied in all directions while adding 1 nm of vacuum perpendicular to the Gr surface. All other parameters used were default settings for the GPAW software.

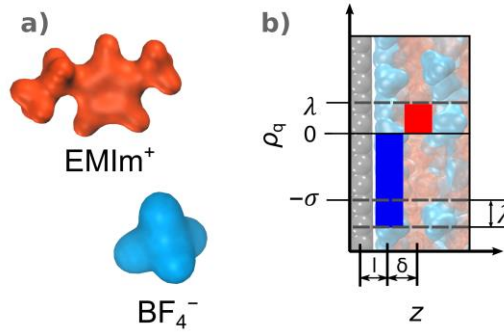


Figure 1. a) The vdW iso-surfaces of simulated IL ions. b) Profiles of the positively charged Gr–EMImBF₄ interface, illustrating the variables of the interfacial bilayer model. Cations and anions are shown with red and blue colors, respectively.

2.2. Evaluation of Potential Drop and Electrolyte Capacitance

To evaluate the contributions of Gr and IL to the potential drop and interfacial capacitance, we divided the interface into the electrolyte and electrode components. The electric potential ($\varphi(z)$) of the IL due to non-uniform distribution of ions at distance z from the electrode surface was found for each replica of a simulated T and σ by integrating the Poisson equation:

$$\varphi(z) = -\frac{z\sigma}{\epsilon\epsilon_0} - \frac{1}{\epsilon\epsilon_0} \int_0^z (z-z')\rho_q(z')dz', \quad (1)$$

where σ is the surface charge density, $\rho_q(z')$ IL charge density at a distance z' from the electrode averaged over trajectory snapshots. ϵ_0 is the permittivity of vacuum, and ϵ is the high-frequency permittivity describing only the electronic polarization.

The potential drop (φ_{IL}) in the IL electrolyte due to non-uniform distribution of ions at the electrode–IL interface was estimated as:

$$\varphi_{\text{IL}} = \varphi_{\text{electrode}} - \varphi_{\text{electrolyte}}, \quad (2)$$

where $\varphi_{\text{electrode}}$ and $\varphi_{\text{electrolyte}}$ are electric potentials at the electrode surface and in the IL bulk, respectively. In the following analyses, instead of the φ_{IL} , relative potential (U) was used:

$$U = \bar{\varphi}_{\text{IL}} - \bar{\varphi}_{\text{PZC}}, \quad (3)$$

where $\bar{\varphi}_{\text{IL}}$ is the mean average potential drop of all simulated replicas and $\bar{\varphi}_{\text{PZC}}$ is the mean average potential of zero charge (PZC).

The electrolyte capacitance (C_{IL}) was evaluated as:

$$C_{\text{IL}} = \frac{d\sigma}{dU}. \quad (4)$$

To smooth the interpolated σ – U dependence, the convolution smoothing with a Hamming window function with a window size of $12 \mu\text{C cm}^{-2}$ was used. The positive and negative aspects of this smoothing method are discussed in Ref. [57].

For the estimation of electrode quantum capacitance (C_{Q}), the σ at Gr electric potential (φ_{Gr}), was calculated as:

$$\sigma = e \int_{-\infty}^{\infty} D(\varepsilon) [f(\varepsilon, T) - f(\varepsilon - e\varphi_{\text{Gr}}, T)] d\varepsilon, \quad (5)$$

where $D(\varepsilon)$ is the Gr DOS, and $f(\varepsilon, T)$ is the Fermi–Dirac distribution function at the given T and electronic energy level ε , shifted relative to Gr Fermi level (E_{F}). The value of φ_{Gr} was estimated from DOS by $\varphi_{\text{Gr}} = (\varepsilon - E_{\text{F}})/e$. Then, C_{Q} was calculated as:

$$C_{\text{Q}} = \frac{d\sigma}{d\varphi_{\text{Gr}}}, \quad (6)$$

using convolution smoothing with a smaller window size of $1.25 \mu\text{C cm}^{-2}$ to avoid oversmoothing the capacitance minima at $\varphi_{\text{Gr}} = 0 \text{ V}$.

The total interfacial capacitance (C_{tot}) was evaluated in terms of electrolyte and electrode capacitances for a given σ value, similarly to capacitors in series:

$$1/C_{\text{tot}} = 1/C_{\text{IL}} + 1/C_{\text{Gr}}. \quad (7)$$

The obtained C_{tot} was plotted on the overall potential drop (U') scale that was calculated as the sum of the electrode potential and the electrolyte potential drop for a given σ value: $U' = U + \varphi_{\text{Gr}}$. Let us note that similar expressions were used to explain experimental results, although in some cases by not evaluating the potential drops, and thus capacitance, within the electrode and electrolyte independently [58].

To investigate changes in the arrangement of interfacial ions at different T and U values, we constructed the number density profiles of the ions in a direction perpendicular to the Gr surface. Furthermore, for better distinguishment between the centers of the interfacial layers, when constructing the number density profiles, the center of the imidazole ring and the location of the boron atom were considered as the positions of the cation and anion, respectively.

2.3. Interfacial bilayer model

The layered interfacial structure of IL allows viewing the oppositely charged IL layers as series-connected capacitors [59]. By considering only the first two IL layers to have a significant effect on the φ_{IL} , then it can be estimated using the interfacial bilayer (IBL) model [60], which defines it as:

$$\varphi_{\text{IL}} \approx \frac{l\sigma - \delta\lambda}{\epsilon\epsilon_0}. \quad (8)$$

The C_{IL} [57]:

$$C_{\text{IL}} = \frac{d\sigma}{dU} = \frac{d\sigma}{d\varphi_{\text{IL}}} \approx \frac{\epsilon\epsilon_0}{l} + \frac{\epsilon\epsilon_0 U - \delta\lambda}{l^2} \cdot \nabla l + \frac{\delta}{l} \nabla \lambda + \frac{\lambda}{l} \nabla \delta, \quad (9)$$

which can be simplified by assuming $l = \text{const}$:

$$C_{\text{IL}} \approx \frac{\epsilon\epsilon_0}{l} + \frac{\delta}{l} \nabla \lambda + \frac{\lambda}{l} \nabla \delta, \quad (10)$$

where $\nabla = \frac{d}{dU}$ (partial derivative), l and δ are the distances between the electrode and the first IL layer and between the first and second IL layers, as illustrated in Fig. 1b. λ describes the excess charge of the first IL layer that overscreens σ . The first term in Eqs. 9–10 is the Helmholtz capacitance:

$$C_H = \frac{\epsilon\epsilon_0}{l}. \quad (11)$$

Eqs. 9 and 10 are suitable for the semi-qualitative description of various interfacial phenomena [20,23,57,61,62] including the $C_{IL}(U)$ dependence.¹ First, the capacitance peak (C_P) is related to the maximal $\nabla\lambda$ value in the vicinity of the PZC. When considering the changes in the positions of the first two that are of IL layers negligible ($\nabla l = 0$ and $\nabla\delta = 0$) and considering the electroneutrality (as $\sigma = \lambda/(\beta-1)$), then Eqs. 8 and 9 give:

$$U_P \approx \frac{l-\delta(\beta-1)}{\epsilon\epsilon_0} \sigma - \varphi_{PZC}, \quad (12)$$

and

$$C_P \approx \frac{\epsilon\epsilon_0}{l-\delta(\beta-1)} = \frac{l}{l-\delta(\beta-1)} C_H = bC_H. \quad (13)$$

The last equation implies that the capacitance peak can be related to the overscreening (in terms of δ and β). The formula can be simplified further by taking $\beta = 2$, i.e., assuming that the maximal $\nabla\lambda$ value is achieved when the ion exchange happens *via* desorbing one co-ion and adsorbing one counter-ion while changing the surface charge by one ion-charge per area [64,65]:

$$C_P \approx \frac{\epsilon\epsilon_0}{l-\delta} = \frac{l}{l-\delta} C_H. \quad (14)$$

Second, at the saturation potential (U_S), the saturation of the second layer of co-ions take place, when $\nabla l = 0$, $\nabla\delta = 0$, and $\nabla\lambda = 0$ [57]:

$$C_S \approx \frac{\epsilon\epsilon_0}{l} = C_H. \quad (15)$$

Below, we discuss the saturation phenomenon in more detail.

Finally, at the monolayer formation potential (U_M), the first layer completely screens the surface charge. Assuming that the screening at that point is Helmholtz-like, the capacitance at U_M equals [57]:

$$C_M \approx \frac{\epsilon\epsilon_0}{l+\delta} = \frac{l}{l+\delta} C_H = aC_H, \quad (16)$$

¹ For electrodes with a limited number of electronic states near the Fermi level (like graphene), the contribution of C_Q must be added to the model [63].

where, in the crowding regime [8], $0.2 \leq a \leq 0.5$ with the lowest and highest values being for the close-packing and inverse-square-root scaling [7], respectively. Furthermore, a scaling relation, arising from the charge conservation law, can be used for the estimation of $C_{\text{IL}}(U)$ dependence [60]:

$$C_{\text{IL}} = a \frac{\epsilon \epsilon_0}{l} \left(\frac{U}{U_{\text{M}}} \right)^{a-1}, \quad (17)$$

where a is the scaling exponent. At $U = U_{\text{M}}$ it simplifies to Eq. 16, and, if $a = 0.5$, it follows the inverse-square-root scaling.

In the studied potential range from -6.5 to 6.5 V, the Gr-EMImBF₄ interface is in the over-screening regime [18,66], as the monolayer formation potential (U_{M}) for EMIm⁺ and BF₄⁻ are -13 V and 20 V, respectively [67]. Accordingly, we focus on the three main variables in Eq. 10 to rationalize the simulated data: Helmholtz capacitance (C_{H}), excess charge density derivative ($\nabla\lambda$), and the layering distance derivative ($\nabla\delta$). C_{H} is defined by the *packing* of counter-ions, $\nabla\lambda$ is dictated by the EDL *charging* via sorption of ions, and $\nabla\delta$ is determined by ion *layering*. Below we present the results using the named concepts along with three characteristic potentials: (1) U_{PZC} when the EDL is overall neutral, (2) U_{S} when the second layer is saturated with co-ions (see Fig. 2), and (3) U_{M} when the first layer is saturated with counter-ions and completely screens the surface charge.

3. Results and discussion

3.1. The effect of electrode potential on electrolyte capacitance

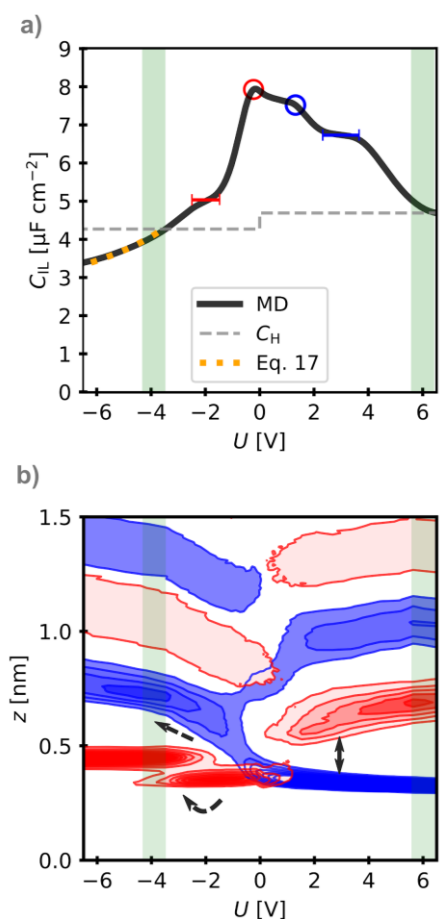


Figure 2. a) Calculated $C_{IL}(U)$ curve for the Gr-EMImBF₄ interface simulated at 450 K. The grey and orange lines show the Helmholtz capacitance (C_H) and the dependence fitted using Eq. 17. The red and blue markers indicate the critical points and plateaus in the $C_{IL}(U)$ dependency. b) The number density $\rho_N(z, U)$ contour maps of EMIm⁺ (red area) and BF₄⁻ (blue area) ions at $T = 450$ K. The interval of contour lines is equal to ρ_{bulk} , with the first contour starting at $1.25\rho_{\text{bulk}}$ and the last contour representing densities higher than $8\rho_{\text{bulk}}$. Arrows mark the potential regions where (1) the layering of IL (bidirectional arrow), (2) the reorientation of cation (curved arrow), and (3) saturation of the second IL layer (straight arrow) occur. Green regions in both figures show the saturation potentials (U_s), where the second IL layer reaches its maximum densities.

Fig. 2 shows the $C_{\text{IL}}(U)$ dependence and the number density contour map that reflects the changes in the EDL structure. We regard the $C_{\text{IL}}(U)$ neither as a camel or bell-shaped but rather as an overlap of two peaks due to the anion and cation adsorption at positive and negative potentials. The overlap of these peaks leads to a wide maximum at the PZC. The arrows in Fig. 2b points to the relations between the anionic and cationic capacitance peaks and the changes of IL structure. These structural changes can be expressed as the maximal values of $\nabla\delta$, $\nabla\lambda$, and ∇l in Eq. 10. Using Eq. 14, we estimated C_{P} near the PZC as $9 \mu\text{F}/\text{cm}^2$ and $7 \mu\text{F}/\text{cm}^2$ at $U = -0.1 \text{ V}$ and 0.1 V , respectively. The evaluated C_{P} values are in relatively good agreement with the calculated $C_{\text{IL}}(U)$ curve in Fig. 2a. Therefore, the IBL model allows making crude estimations of the capacitance peaks.

The C_{IL} is independent of U within -2.5 – -1.5 V and 2 – 4 V , indicated by the two plateaus in the $C_{\text{IL}}(U)$ dependence (see Fig. 2a). At negative potentials, the density contours indicate the reorientation of EMIm^+ ions between parallel and perpendicular directions relative to the Gr surface. Some aspects of such reorientation are discussed in Refs. [68–70]. As in previous works [41,43], with the reorientation of cations upon surface charging, δ remained almost the same. In this work, we note that upon surface charging l effectively increases (see Fig. 2b). Within a specific U range, the first two terms in Eq. 9 balance for the change of l . That results in an apparently constant C_{IL} value around -2 V .

As shown in Fig. 2b and Fig. S1, a similar compensating effect occurs around 3 V . The mechanism is slightly different. Here, due to the smaller size of ions, a relatively low counter-ion density is required to overscreen the surface charge. That leaves voids on the electrode surface, which are filled with cations, as shown for the U values 1.5 V ($12 \mu\text{C cm}^{-2}$) and 2.1 V ($16 \mu\text{C cm}^{-2}$) in Fig. S2. Upon further surface charging, the first IL layer becomes denser, and the cations or their alkyl chains can no longer settle in the voids of the first layer. That causes a more significant separation of the two oppositely charged IL layers and the increase of $\nabla\delta$. Meanwhile, the number of co-ions in the second IL layer does not significantly increase (see SI Fig. S1b), indicating the decrease of $\nabla\lambda$ and leading to

a constant C_{IL} value in the U range of 2–4 V. In our previous work [57], a similar mechanism resulted in a capacitance peak caused by the BMIm⁺ reorientation.

Fig. 2b shows that the second layer has its maximal density at –4 V and 6 V. These are the saturation potential (U_{S}) for co-ions in the EDL structure. At absolute potentials larger than $|U_{\text{S}}|$, the capacitance curve follows Eq. 17 [60] with fitted a values of 0.58 (for $U < -4$ V, see Fig. 2a) and 0.81 (for $U > 6$ V). In additional MD simulations (see Appendix 3), we estimated the C_{H} values of 4.3 $\mu\text{F}/\text{cm}^2$ (for Gr-EMIm⁺ interface) and 4.7 $\mu\text{F}/\text{cm}^2$ (for Gr-BF₄⁻ interface). Fig. 2a highlights a reasonably precise intersection of vertical lines (U_{S}) and the dashed line (C_{H}) with the calculated $C(U)$ curve. That is expected from the IBL model (Eqs. 9 and 15) assuming $\nabla l = 0$, $\nabla \delta = 0$, and $\nabla \lambda = 0$, because the latter condition expresses the saturation. Moreover, the IBL model enables estimating the combining U_{S} by combining Eqs. 15 and 17:

$$U_{\text{S}} = U_{\text{M}} \left(\frac{1}{a} \right)^{1/(a-1)}, \quad (18)$$

The evaluated values of –3.5 V and 6.5 V are in an acceptable agreement with the simulation results from Fig. 2, where the saturation is seen around –4 V and 6 V, respectively.

As shown, the IBL model consistently interprets the calculated $C_{\text{IL}}(U)$ dependency. Namely, the following $C_{\text{IL}}(U)$ features are seen in Figure 2a: (1) $C_{\text{IL}} \approx aC_{\text{H}}(U/U_{\text{M}})^{a-1}$ scaling at $U < -4$ V (Eqs. 16–18), (2) $C_{\text{IL}} \approx C_{\text{H}}$ at the saturation potential (Eq. 15), (3) plateaus around –2 and 3 V, (4) $C_{\text{P}} \approx bC_{\text{H}}$ at the peak potential (Eq. 13–14).

3.2. The effect of temperature on the electrolyte capacitance

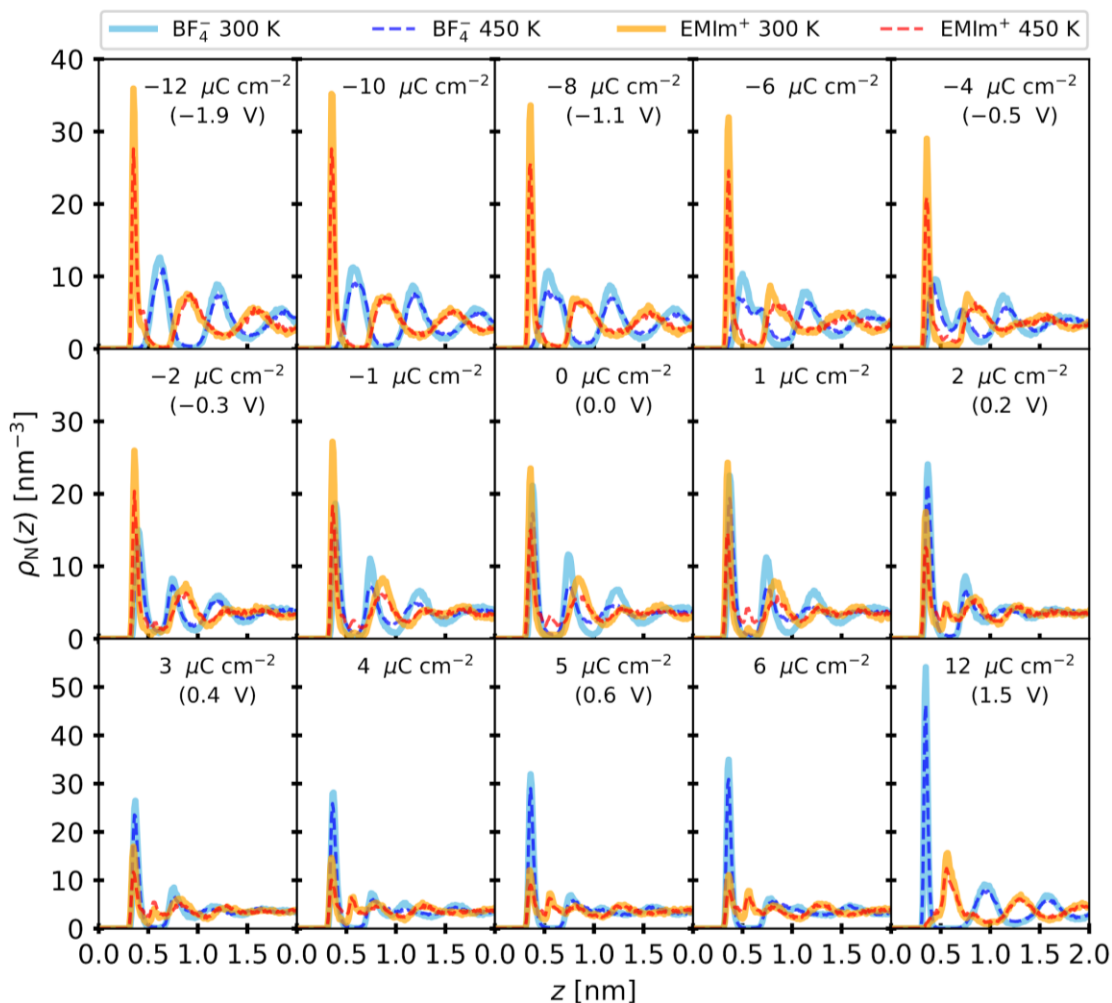


Figure 3. Number density profiles of EMIm⁺ and BF₄⁻ ions in the case of the U range from -1.9 to 1.5 V at T values 300 K and 450 K. The potential U values are given for 450 K.

Fig. 3 illustrates the changing of the Gr-EMImBF₄ interfacial structure in the U range from -1.9 to 1.5 V. The IL has a layered structure at the interface. The layers contain approximately equal amounts of anions and cations even at the PZC. The formation of a layered structure is caused by the interaction of ions with Gr, which prevents the ions from packing similarly to the bulk IL. As the electrode is charged, co-ions are pushed away from the surface to the second layer. That can be seen in Fig. 3 by comparing the profiles of U values -0.5 and -1.1 V as well as 0.0 and 0.2 V. Despite the

electrostatic repulsion between the electrode and co-ions, the first IL layer contains a significant number of co-ions at small $|U|$, enabled by ion–ion correlation and the voids on the electrode surface that are large enough to accommodate co-ions.

Temperature affects the capacitance foremost near the PZC, as shown in Fig. 4. Within $-0.5-2$ V, when the T increases, the values of C_{IL} peaks decrease, and the separation between two local capacitance peaks increases. When comparing the number density profiles of T equals 300 K and 450 K in Fig. 3, it can be seen that the increased thermal motion leads to changes in the IL interfacial structure. On the one hand, the position of the number density peaks remains the same. On the other hand, all peaks are smeared due to thermal motion – their heights are shortened, and widths are broadened. Thus, we may assume that l and δ in the IBL model do not depend on the T , while β and λ do. That means the thermal motion foremost diminishes overscreening and decreases the maximal excess charge density. These structural changes translate into a particular $C(U, T)$ dependence.

According to Eqs. 12 and 13, with the decrease of β , the peak absolute potential (U_p) value increases, while the capacitance peak (C_p) value decreases, resulting in $dC/dT < 0$. Fig. 4 illustrates the same trends in the MD simulations. The reader can mark the $|U_p|$ increase (especially on the positive side), and the C_p decreases, decrease with the increase of T . Note how the shifting of U_p to higher absolute potentials uncovers regions (for example, around 1–2 V) where $dC/dT > 0$. That leads us to the essential question of choosing the proper reference for the dC/dT comparison. One can choose between arbitrary U or σ values and compare differential and integral capacitances, like in Ref. [41]. On top of that, there are fast and slow capacitive processes [71], which analysis requires investigating the impedance spectra. Considering all this, we suggest using characteristic potentials such as U_M , U_S , or U_p . From Eqs. 10 and assuming l and δ are independent of U and T , it is straightforward to express the $C(T)$ dependencies at these characteristic potentials:

$$\frac{dC_M}{dT} \approx 0, \frac{dC_S}{dT} \approx 0, \text{ and } \frac{dC_p}{dT} \approx \frac{\delta}{l} \frac{d\beta}{dT} \quad (19)$$

The first potential (U_M) [66], is hardly achievable in experiments [72]. Moreover, it is independent of the T , as the strength of electrostatic electrode–ion interactions exceed the thermal energy at high $|U|$. The second potential (U_S) can possibly be probed with atomic force microscopy and X-ray reflectivity measurements, yet it is independent of T according to Eqs. 15 and 19. The last potential (U_P) is most easily identified in experiments, simulations, and theory as a striking $C(U)$ curve feature. Focusing on U_P has the advantage of linking the $C(U, T)$ dependence to the EDL charging mechanism in terms of *packing* (C_H), *layering* ($\nabla\delta$), and *charging* ($\nabla\lambda$). Herewith, choosing an arbitrary constant U value may lead to wrong conclusions. For example, it would be ungrounded to relate the positive dependence within 1–2 V from Fig. 4 to the anomalous capacitance concept from the works by Boda *et al.* [30–32]. Therefore, we propose focusing on dC_P/dT at U_P to avoid misinterpretations. In this study, the λ and, accordingly, C_P values decreased with temperature resulting in $dC_P/dT < 0$ (see Fig. 4).

Qualitatively the results of our simulations resemble the experiments of Drüscher *et al.* [38] with BMPyrFAP IL at Au(111) electrode. First, they also observed a wide capacitance peak that we interpret as overlapping anionic and cationic peaks. Second, the capacitance peak value decreased with increasing temperature ($dC_P/dT < 0$). Third, similarly to Fig. 4, their anionic peak shifted when increasing T . The latter resulted in both $dC/dT < 0$ and $dC/dT > 0$ being observed in different U regions. These complex results described the *fast capacitive process* of restoring electroneutrality upon potential variation. The *slow capacitive process* was characterized by $dC/dT < 0$ at all studied potentials, and it has not been captured in the presented simulations of the Gr–EMImBF₄ interface. Experimental results suggest that the slow process may be related to the reorientation of strongly bound ions. Thus, in principle, it could be observed around –3 V for the Gr–EMImBF₄ interface if it is studied with considerably longer non-equilibrium MD simulations, which allow investigating the dynamic processes occurring at the interface [68]. Drüscher *et al.* [38] likewise pointed out that the

differentiation between the slow and fast processes is essential in understanding the $C(U, T)$ dependence. Due to the lack of such analysis in other experimental works, we refer to their discussion in Ref. [61] and overlook the so-called anomalous dependence ($dC/dT > 0$) [73].

Previous computational works, relying on MD simulations, reported in [41,43,74,75], confirm our observations that the T increase does not induce any significant separation of IL layers nor peak positions changes in the density profiles. Concurrently, the T increase shortens and widens the number density peaks. $C(U)$ curves at different T from Refs. [39–41] display the same features as reported in this work, albeit in a narrower studied potential range. Namely, $dC_P/dT < 0$ near the PZC, the shift of U_P to higher absolute potentials, and ranges with $dC/dT > 0$. Chen *et al.* [40] describe the separation of capacitance peaks as the transformation of $C(U)$ from camel to bell shape within the modified mean-field theory. Shen *et al.* [42] studied the same Gr-EMImBF₄ interface with classical DFT and observed similar features of the $C(U, T)$ dependence as in this study: $dC_P/dT < 0$; U ranges with $dC/dT > 0$; and shift of U_P upon heating. These and other authors [76] referred to the idea of ion association that weakens with increasing T . It may be speculated that the observed changes in overscreening (β), saturation (λ), reorientation and layering (δ) are also related to the electrode–ion and ion–ion correlation affected by T . Thus, we find that the proposed IBL model-based explanation of the U_P shift and $dC_P/dT < 0$ is complementary to both theoretical explanations [40] and phenomenological reasoning [39,41] of the $C(U, T)$ dependence.

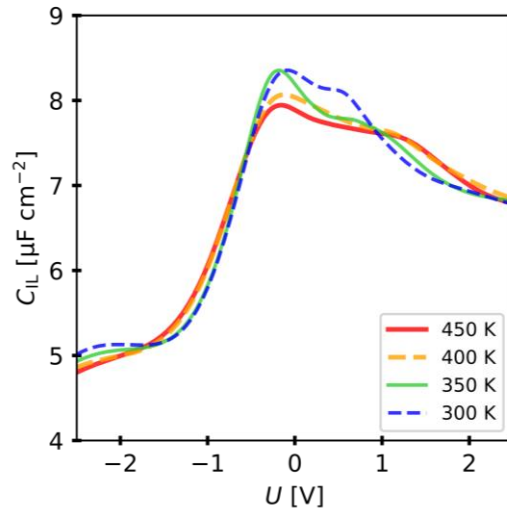


Figure 4. Gr-EMImBF₄ interface $C_{iL}(U)$ dependencies for simulated T values in the potential range from -2.5 to 2.5 V. The potential axis (U) accounts for the shift due to ϕ_{PZC} of each studied T . The average values of the ϕ_{PZC} were 0.17 V, 0.14 V, 0.13 V, and 0.11 V at 300 K, 350 K, 400 K, and 450 K, respectively.

3.3. The effect of temperature and quantum capacitance on interfacial capacitance

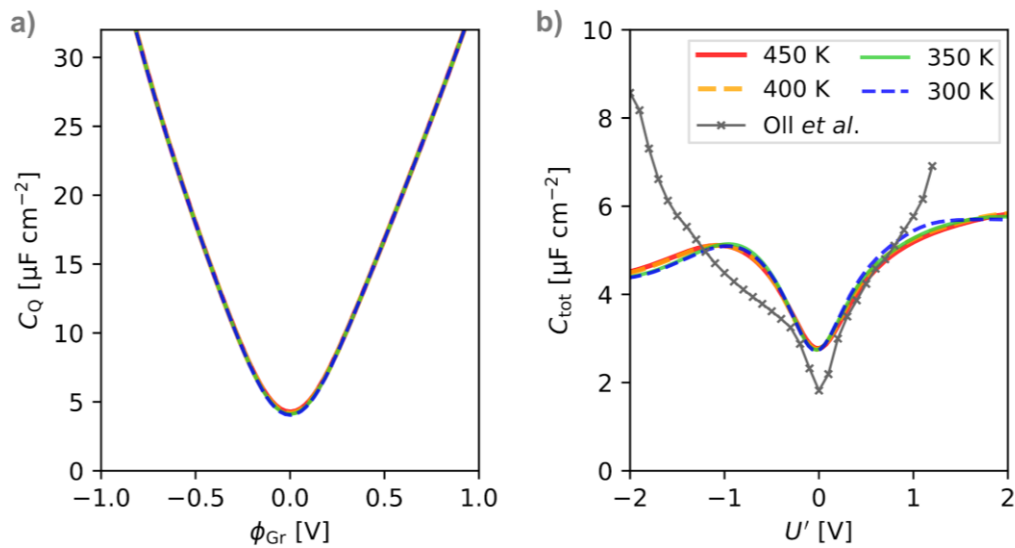


Figure 5. a) $C_Q(\phi_{Gr})$ dependencies for simulated temperatures. b) $C_{tot}(U')$ dependencies for simulated temperatures along with the experimental data reported by Oll *et al.* [16]. The potentials of experimental results by Oll *et al.* are shifted by the PZC.

A notable potential drop within the Gr is observed due to significant shifting of the Fermi level, caused by the low density of states near the latter. Fig. 5a shows the calculated quantum capacitance (C_Q) with a characteristic V shape in agreement with the experimental results reported by Xia *et al.* [77] and Fang *et al.* [78]. Furthermore, Fig. 5 highlights the negligible effect of T on the C_Q . When comparing the C_Q and C_{IL} values near the PZC, C_Q is almost two times lower and therefore limits the total interfacial capacitance, shown in Fig. 5b. As the C_Q has a substantial effect on the C_{tot} within the U' range from -1 V to 1 V, where the $C_{tot}(U')$ curve has a minimum in contrast to the $C_{IL}(U)$ maxima. Thus, as the C_Q is only slightly affected by the T , the heating of the studied system has a minor effect on C_{tot} in the studied T range.

The impact of C_Q on C_{tot} of Gr-BMImPF₆ interface was previously studied with MD simulations in combination with DFT calculations by Paek *et al.* [79], where the limiting effect of C_Q on C_{tot} was also demonstrated. However, the effect was not as drastic, due to lower $C_{IL}(U)$ maxima. For the Gr-EMImBF₄ interface, a similar trend was reported by Zhan *et al.* [63], who used a coarse-grained model of EMImBF₄. Experimentally, using electrochemical impedance spectroscopy, the Gr-EMImBF₄ interface was studied by Oll *et al.* [16], who showed that interfacial $C(U)$ dependence has a minimum near the PZC. As shown in Fig. 5b, within the U' range from -1 V to 1 V, their reported $C(U)$ dependence is in accordance with our simulations. The experimental curve lacks a “shoulder” around -1 V and at higher absolute potentials exceeds our estimated $C(U)$ values. The deviation may be caused by several approximations used in the MD simulations and analysis, such as (1) simplistic electrode model, (2) simplistic electronic polarization model, and (3) poor sampling. The straightforward way of addressing all these issues is in running longer simulations with constant potential methods and polarizable force fields [21,80–83]. That way has been recently opened due to software development, force field derivation, and DFT-based MD reference simulations [25,26,82,84–86]. We proceed with it to obtain models reproducing experimental results.

4. Conclusions

In this study, we modeled graphene–ionic liquid (IL = EMImBF₄) interfacial structure and capacitance (C) dependence on potential (U) and temperature (T). We have defined three structure-determined potentials (U_M , U_S , and U_P) to interpret the simulated $C(U, T)$ curves using the original interfacial bilayer model. The maximal density of counter-ions of the first layer and co-ions of the second layer is reached at U_M and U_S , respectively. The capacitance peak potential (U_P) corresponds to a state when the excess charge density derivative ($\nabla\lambda$) is at the maximum. For these potentials, the interfacial bilayer model approximates $C(U, T)$ as:

$$C_P \approx \frac{l}{l-\delta} C_H \text{ and } \frac{dC_P}{dT} \approx \frac{\delta}{l} \frac{d\nabla\lambda}{dT},$$

$$C_S \approx C_H \text{ and } \frac{dC_S}{dT} \approx 0,$$

$$C_M \approx \frac{l}{l+\delta} C_H \text{ and } \frac{dC_M}{dT} \approx 0,$$

where l and δ are the distances between the electrode and the first IL layer and between the first and second IL layers, and C_H is the Helmholtz capacitance. We suggest using the capacitance peak potential (U_P) for analyzing the $C(T)$ dependence. That allows linking structural changes with interfacial properties. For instance, we observed negative dependence ($dC_P/dT < 0$) and showed its correlation to excess charge density (λ) decrease with increasing T .

In essence, the listed equations relate the geometry (l , δ) with the capacitance without any empirical parameters. However, the underlying model requires a correction for the electronic density distribution in the electrode material. We have shown that accounting for the contribution of graphene to the total interfacial capacitance (C_{tot}) dampens the T influence and leads to an encouraging agreement with the experimental $C(U)$ curve.

Acknowledgments

This work was supported by the Estonian Research Council grant PSG249 and by the EU through the European Regional Development Fund under project TK141 (2014-2020.4.01.15-0011). The financial support from FCT/MCTES through the Portuguese national funds, project No. UID/QUI/50006/2021 (LAQV@REQUIMTE) is also acknowledged. For providing us with the computational resources, we would like to recognize the Partnership for Advanced Computing in Europe (PRACE), the Distributed European Computing Initiative (DECI), and the HPC Center of the University of Tartu.

References

- [1] M.V. Fedorov, A.A. Kornyshev, Ionic liquids at electrified interfaces, *Chem. Rev.* 114 (2014) 2978–3036. <https://doi.org/10.1021/cr400374x>.
- [2] D.R. MacFarlane, N. Tachikawa, M. Forsyth, J.M. Pringle, P.C. Howlett, G.D. Elliott, J.H. Davis, M. Watanabe, P. Simon, C.A. Angell, Energy applications of ionic liquids, *Energy Environ. Sci.* 7 (2014) 232–250. <https://doi.org/10.1039/C3EE42099J>.
- [3] G. Chatel, D.R. MacFarlane, Ionic liquids and ultrasound in combination: synergies and challenges, *Chem. Soc. Rev.* 43 (2014) 8132–8149. <https://doi.org/10.1039/C4CS00193A>.
- [4] U. Kosidlo, M. Omastová, M. Micusík, G. Ćirić-Marjanović, H. Randriamahazaka, T. Wallmersperger, A. Aabloo, I. Kolaric, T. Bauernhansl, Nanocarbon based ionic actuators—a review, *Smart Mater. Struct.* 22 (2013) 104022. <https://doi.org/10.1088/0964-1726/22/10/104022>.
- [5] M. Watanabe, M.L. Thomas, S. Zhang, K. Ueno, T. Yasuda, K. Dokko, Application of Ionic Liquids to Energy Storage and Conversion Materials and Devices, *Chem. Rev.* 117 (2017) 7190–7239. <https://doi.org/10.1021/acs.chemrev.6b00504>.
- [6] Y. Zhao, T. Bostrom, Application of Ionic Liquids in Solar Cells and Batteries: A Review, *Curr. Org. Chem.* 19 (2015) 556–566.
- [7] A.A. Kornyshev, Double-Layer in Ionic Liquids: Paradigm Change?, *J. Phys. Chem. B.* 111 (2007) 5545–5557. <https://doi.org/10.1021/jp067857o>.
- [8] M.Z. Bazant, B.D. Storey, A.A. Kornyshev, Double Layer in Ionic Liquids: Overscreening versus Crowding, *Phys. Rev. Lett.* 106 (2011) 046102. <https://doi.org/10.1103/PhysRevLett.106.046102>.
- [9] Z.A.H. Goodwin, G. Feng, A.A. Kornyshev, Mean-Field Theory of Electrical Double Layer In Ionic Liquids with Account of Short-Range Correlations, *Electrochimica Acta.* 225 (2017) 190–197. <https://doi.org/10.1016/j.electacta.2016.12.092>.
- [10] A. Yochelis, Spatial Structure of Electrical Diffuse Layers in Highly Concentrated Electrolytes: A Modified Poisson–Nernst–Planck Approach, *J. Phys. Chem. C.* (2014) DOI: 10.1021/jp412616f. <https://doi.org/10.1021/jp412616f>.
- [11] A.C. Maggs, R. Podgornik, General theory of asymmetric steric interactions in electrostatic double layers, *Soft Matter.* (2016). <https://doi.org/10.1039/C5SM01757B>.

- [12] B. Skinner, T. Chen, M.S. Loth, B.I. Shklovskii, Theory of volumetric capacitance of an electric double-layer supercapacitor, *Phys. Rev. E.* 83 (2011) 056102. <https://doi.org/10.1103/PhysRevE.83.056102>.
- [13] K. Ma, J. Forsman, C.E. Woodward, A Classical Density Functional Study of Clustering in Ionic Liquids at Electrified Interfaces, *J. Phys. Chem. C.* 121 (2017) 1742–1751. <https://doi.org/10.1021/acs.jpcc.6b11491>.
- [14] Y.-Z. Su, Y.-C. Fu, J.-W. Yan, Z.-B. Chen, B.-W. Mao, Double Layer of Au(100)/Ionic Liquid Interface and Its Stability in Imidazolium-Based Ionic Liquids, *Angew. Chem. Int. Ed.* 48 (2009) 5148–5151. <https://doi.org/10.1002/anie.200900300>.
- [15] R. Atkin, N. Borisenko, M. Drüschler, S.Z. El Abedin, F. Endres, R. Hayes, B. Huber, B. Røling, An in situ STM/AFM and impedance spectroscopy study of the extremely pure 1-butyl-1-methylpyrrolidinium tris(pentafluoroethyl)trifluorophosphate/Au(111) interface: potential dependent solvation layers and the herringbone reconstruction, *Phys. Chem. Chem. Phys.* 13 (2011) 6849–6857. <https://doi.org/10.1039/c0cp02846k>.
- [16] O. Oll, T. Romann, C. Siimenson, E. Lust, Influence of chemical composition of electrode material on the differential capacitance characteristics of the ionic liquid|electrode interface, *Electrochem. Commun.* 82 (2017) 39–42. <https://doi.org/10.1016/j.elecom.2017.07.015>.
- [17] R. Costa, I.V. Voroshylova, M.N.D.S. Cordeiro, C.M. Pereira, A.F. Silva, Enhancement of differential double layer capacitance and charge accumulation by tuning the composition of ionic liquids mixtures, *Electrochimica Acta.* 261 (2018) 214–220. <https://doi.org/10.1016/j.electacta.2017.12.134>.
- [18] M.V. Fedorov, A.A. Kornyshev, Towards understanding the structure and capacitance of electrical double layer in ionic liquids, *Electrochimica Acta.* 53 (2008) 6835–6840. <https://doi.org/10.1016/j.electacta.2008.02.065>.
- [19] C. Merlet, D.T. Limmer, M. Salanne, R. van Roij, P.A. Madden, D. Chandler, B. Rotenberg, The Electric Double Layer Has a Life of Its Own, *J. Phys. Chem. C.* 118 (2014) 18291–18298. <https://doi.org/10.1021/jp503224w>.
- [20] I.V. Voroshylova, M. Leminen, H. Ers, M. Mišin, V.A. Koverga, C.M. Pereira, V.B. Ivaništšev, M.N.D.S. Cordeiro, On the role of the surface charge plane position at Au(hkl)-BMImPF6 interfaces, *Electrochimica Acta.* 318 (2019) 76–82. <https://doi.org/10.1016/j.electacta.2019.05.058>.
- [21] D. Bedrov, J.-P. Piquemal, O. Borodin, A.D. MacKerell, B. Roux, C. Schröder, Molecular Dynamics Simulations of Ionic Liquids and Electrolytes Using Polarizable Force Fields, *Chem. Rev.* 119 (2019) 7940–7995. <https://doi.org/10.1021/acs.chemrev.8b00763>.
- [22] M. Wu, W. Li, S. Li, G. Feng, Capacitive performance of amino acid ionic liquid electrolyte-based supercapacitors by molecular dynamics simulation, *RSC Adv.* 7 (2017) 28945–28950. <https://doi.org/10.1039/C7RA00443E>.
- [23] I.V. Voroshylova, H. Ers, B. Docampo-Álvarez, P. Pikma, V.B. Ivaništšev, M.N.D.S. Cordeiro, Hysteresis in the MD Simulations of Differential Capacitance at the Ionic Liquid–Au Interface, *J. Phys. Chem. Lett.* (2020) 10408–10413. <https://doi.org/10.1021/acs.jpcllett.0c03212>.
- [24] H. Valencia, M. Kohyama, S. Tanaka, H. Matsumoto, First-Principles Study of EMIM-FAFSA Molecule Adsorption on a Li(100) Surface as a Model for Li-Ion Battery Electrodes, *J. Phys. Chem. C.* 116 (2012) 8493–8509. <https://doi.org/10.1021/jp2109797>.
- [25] E. Paek, A.J. Pak, G.S. Hwang, On the influence of polarization effects in predicting the interfacial structure and capacitance of graphene-like electrodes in ionic liquids, *J. Chem. Phys.* 142 (2015) 024701–6. <https://doi.org/10.1063/1.4905328>.
- [26] H. Ers, M. Leminen, M. Mišin, A.P. Seitsonen, M.V. Fedorov, V.B. Ivaništšev, Graphene–Ionic Liquid Interfacial Potential Drop from Density Functional Theory-Based Molecular Dynamics Simulations, *J. Phys. Chem. C.* 124 (2020) 19548–19555. <https://doi.org/10.1021/acs.jpcc.0c02964>.

- [27] L. Scalfi, M. Salanne, B. Rotenberg, Molecular Simulation of Electrode-Solution Interfaces, *Annu. Rev. Phys. Chem.* 72 (2021) 189–212. <https://doi.org/10.1146/annurev-physchem-090519-024042>.
- [28] T. Dufils, G. Jeanmairet, B. Rotenberg, M. Sprik, M. Salanne, Simulating Electrochemical Systems by Combining the Finite Field Method with a Constant Potential Electrode, *Phys. Rev. Lett.* 123 (2019). <https://doi.org/10.1103/PhysRevLett.123.195501>.
- [29] C. Zhan, C. Lian, Y. Zhang, M.W. Thompson, Y. Xie, J. Wu, P.R.C. Kent, P.T. Cummings, D. Jiang, D.J. Wesolowski, Computational Insights into Materials and Interfaces for Capacitive Energy Storage, *Adv. Sci.* 4 (2017) 1700059. <https://doi.org/10.1002/advs.201700059>.
- [30] M. Holovko, V. Kapko, D. Henderson, D. Boda, On the influence of ionic association on the capacitance of an electrical double layer, *Chem. Phys. Lett.* 341 (2001) 363–368. [https://doi.org/10.1016/S0009-2614\(01\)00505-X](https://doi.org/10.1016/S0009-2614(01)00505-X).
- [31] D. Boda, D. Henderson, The capacitance of the solvent primitive model double layer at low effective temperatures, *J. Chem. Phys.* 112 (2000) 8934–8938.
- [32] D. di Caprio, J. Stafiej, Z. Borkowska, Anomalous temperature dependence of differential capacity at an uncharged interface with Debye–Hückel electrolyte: Field theoretical approach, *J. Electroanal. Chem.* 582 (2005) 41–49. <https://doi.org/10.1016/j.jelechem.2005.02.008>.
- [33] L. Siinor, R. Arendi, K. Lust, E. Lust, Influence of temperature on the electrochemical characteristics of Bi(111)|ionic liquid interface, *J. Electroanal. Chem.* 689 (2013) 51–56. <https://doi.org/10.1016/j.jelechem.2012.11.018>.
- [34] F. Silva, C. Gomes, M. Figueiredo, R. Costa, A. Martins, C.M. Pereira, The electrical double layer at the [BMIM][PF₆] ionic liquid/electrode interface: Effect of temperature on the differential capacitance, *J. Electroanal. Chem.* 622 (2008) 153–160.
- [35] V. Ivaništšev, A. Ruzanov, K. Lust, E. Lust, Comparative Impedance Study of Cd(0001) Electrode in EMImBF₄ and KI Aqueous Solution at Different Temperatures, *J. Electrochem. Soc.* 160 (2013) H368–H375. <https://doi.org/10.1149/2.129306jes>.
- [36] C. Gomes, R. Costa, C.M. Pereira, A.F. Silva, The electrical double layer at the ionic liquid/Au and Pt electrode interface, *RSC Adv.* 4 (2014) 28914–28921. <https://doi.org/10.1039/C4RA03977G>.
- [37] V. Lockett, M. Horne, R. Sedev, T. Rodopoulos, J. Ralston, Differential capacitance of the double layer at the electrode/ionic liquids interface, *Phys. Chem. Chem. Phys.* 12 (2010) 12499–12512. <https://doi.org/10.1039/c0cp00170h>.
- [38] M. Drüschler, N. Borisenko, J. Wallauer, C. Winter, B. Huber, F. Endres, B. Roling, New insights into the interface between a single-crystalline metal electrode and an extremely pure ionic liquid: slow interfacial processes and the influence of temperature on interfacial dynamics, *Phys. Chem. Chem. Phys.* 14 (2012) 5090–5099.
- [39] J. Vatamanu, L. Xing, W. Li, D. Bedrov, Influence of temperature on the capacitance of ionic liquid electrolytes on charged surfaces., *Phys. Chem. Chem. Phys.* 16 (2014) 5174–5182. <https://doi.org/10.1039/c3cp54705a>.
- [40] M. Chen, Z.A.H. Goodwin, G. Feng, A.A. Kornyshev, On the temperature dependence of the double layer capacitance of ionic liquids, *J. Electroanal. Chem.* 819 (2018) 347–358. <https://doi.org/10.1016/j.jelechem.2017.11.005>.
- [41] X. Liu, Y. Han, T. Yan, Temperature Effects on the Capacitance of an Imidazolium-based Ionic Liquid on a Graphite Electrode: A Molecular Dynamics Simulation, *ChemPhysChem.* 15 (2014) 2503–2509. <https://doi.org/10.1002/cphc.201402220>.
- [42] G. Shen, Y. Sun, Y. Wang, X. Lu, X. Ji, Interfacial structure and differential capacitance of ionic liquid/graphite interface: A perturbed-chain SAFT density functional theory study, *J. Mol. Liq.* 310 (2020) 113199. <https://doi.org/10.1016/j.molliq.2020.113199>.
- [43] S.A. Kislenco, R.H. Amirov, I.S. Samoylov, Influence of temperature on the structure and dynamics of the [BMIM][PF₆] ionic liquid/graphite interface, *Phys. Chem. Chem. Phys.* 12 (2010) 11245–11250. <https://doi.org/10.1039/c0cp00220h>.

- [44] L. Martínez, R. Andrade, E.G. Birgin, J.M. Martínez, PACKMOL: A Package for Building Initial Configurations for Molecular Dynamics Simulations, *J. Comput. Chem.* 30 (2009) 2157–2164. <https://doi.org/10.1002/jcc.21224>.
- [45] W.-G. Xu, L. Li, X.-X. Ma, J. Wei, W.-B. Duan, W. Guan, J.-Z. Yang, Density, surface tension, and refractive index of ionic liquids homologue of 1-alkyl-3-methylimidazolium tetrafluoroborate [C_nmim][BF₄](n= 2, 3, 4, 5, 6), *J. Chem. Eng. Data.* 57 (2012) 2177–2184.
- [46] E. Roos Nerut, K. Karu, I.V. Voroshylova, K. Kirchner, T. Kirchner, M.V. Fedorov, V.B. Ivaništšev, NaRiBaS—A Scripting Framework for Computational Modeling of Nanomaterials and Room Temperature Ionic Liquids in Bulk and Slab, *Computation.* 6 (2018) 57. <https://doi.org/10.3390/computation6040057>.
- [47] University of Tartu, UT Rocket, (2018). <https://doi.org/10.23673/PH6N-0144>.
- [48] M.J. Abraham, T. Murtola, R. Schulz, S. Páll, J.C. Smith, B. Hess, E. Lindahl, GROMACS: High performance molecular simulations through multi-level parallelism from laptops to supercomputers, *SoftwareX.* 1–2 (2015) 19–25. <https://doi.org/10.1016/j.softx.2015.06.001>.
- [49] D. Van Der Spoel, E. Lindahl, B. Hess, G. Groenhof, A.E. Mark, H.J.C. Berendsen, GROMACS: Fast, flexible, and free, *J. Comput. Chem.* 26 (2005) 1701–1718. <https://doi.org/10.1002/jcc.20291>.
- [50] J.N. Canongia Lopes, J. Deschamps, A.A.H. Pádua, Modeling Ionic Liquids Using a Systematic All-Atom Force Field, *J. Phys. Chem. B.* 108 (2004) 2038–2047. <https://doi.org/10.1021/jp0362133>.
- [51] G. Bussi, D. Donadio, M. Parrinello, Canonical sampling through velocity rescaling, *J. Chem. Phys.* 126 (2007) 014101. <https://doi.org/10.1063/1.2408420>.
- [52] J.J. Mortensen, L.B. Hansen, K.W. Jacobsen, Real-space grid implementation of the projector augmented wave method, *Phys. Rev. B.* 71 (2005) 035109. <https://doi.org/10.1103/PhysRevB.71.035109>.
- [53] J. Enkovaara, C. Rostgaard, J.J. Mortensen, J. Chen, M. Duřak, L. Ferrighi, J. Gavnholt, C. Glinsvad, V. Haikola, H.A. Hansen, H.H. Kristoffersen, M. Kuisma, A.H. Larsen, L. Lehtovaara, M. Ljungberg, O. Lopez-Acevedo, P.G. Moses, J. Ojanen, T. Olsen, V. Petzold, N.A. Romero, J. Stausholm-Møller, M. Strange, G.A. Tritsarlis, M. Vanin, M. Walter, B. Hammer, H. Häkkinen, G.K.H. Madsen, R.M. Nieminen, J.K. Nørskov, M. Puska, T.T. Rantala, J. Schiøtz, K.S. Thygesen, K.W. Jacobsen, Electronic structure calculations with GPAW: a real-space implementation of the projector augmented-wave method, *J. Phys. Condens. Matter.* 22 (2010) 253202. <https://doi.org/10.1088/0953-8984/22/25/253202>.
- [54] J.P. Perdew, K. Burke, M. Ernzerhof, Generalized Gradient Approximation Made Simple, *Phys. Rev. Lett.* 77 (1996) 3865–3868. <https://doi.org/10.1103/PhysRevLett.77.3865>.
- [55] A.H. Larsen, J.J. Mortensen, J. Blomqvist, I.E. Castelli, R. Christensen, M. Dulak, J. Friis, M.N. Groves, B. Hammer, C. Hargus, E.D. Hermes, P.C. Jennings, P.B. Jensen, J. Kermode, J.R. Kitchin, E.L. Kolsbjerg, J. Kubal, K. Kaasbjerg, S. Lysgaard, J.B. Maronsson, T. Maxson, T. Olsen, L. Pastewka, A. Peterson, C. Rostgaard, J. Schiøtz, O. Schütt, M. Strange, K.S. Thygesen, T. Vegge, L. Vilhelmsen, M. Walter, Z. Zeng, K.W. Jacobsen, The atomic simulation environment—a Python library for working with atoms, *J. Phys. Condens. Matter.* 29 (2017) 273002. <https://doi.org/10.1088/1361-648X/aa680e>.
- [56] H.J. Monkhorst, J.D. Pack, Special points for Brillouin-zone integrations, *Phys. Rev. B.* 13 (1976) 5188–5192. <https://doi.org/10.1103/PhysRevB.13.5188>.
- [57] I.V. Voroshylova, H. Ers, V. Koverga, B. Docampo-Álvarez, P. Pikma, V.B. Ivaništšev, M.N.D.S. Cordeiro, Ionic liquid–metal interface: The origins of capacitance peaks, *Electrochimica Acta.* 379 (2021) 138148. <https://doi.org/10.1016/j.electacta.2021.138148>.
- [58] Md.M. Islam, T. Ohsaka, Model of electrical double layer structure at semi-metallic electrode/ionic liquid interface, *Electrochimica Acta.* 368 (2021) 137555. <https://doi.org/10.1016/j.electacta.2020.137555>.

- [59] G. Feng, J. Huang, B.G. Sumpter, V. Meunier, R. Qiao, A “counter-charge layer in generalized solvents” framework for electrical double layers in neat and hybrid ionic liquid electrolytes, *Phys. Chem. Chem. Phys.* 13 (2011) 14723–14734. <https://doi.org/10.1039/c1cp21428d>.
- [60] V. Ivaništšev, K. Kirchner, T. Kirchner, M.V. Fedorov, Restructuring of the electrical double layer in ionic liquids upon charging, *J. Phys. Condens. Matter.* 27 (2015) 102101. <https://doi.org/10.1088/0953-8984/27/10/102101>.
- [61] V.B. Ivaništšev, K. Kirchner, M.V. Fedorov, Double layer in ionic liquids: capacitance vs temperature, *ArXiv*. (2017) 1711.06854.
- [62] A. Ruzanov, M. Leminen, P. Jakovits, S.N. Srirama, I.V. Voroshylova, M.N.D.S. Cordeiro, C.M. Pereira, J. Rossmeisl, V.B. Ivaništšev, On the thickness of the double layer in ionic liquids, *Phys. Chem. Chem. Phys.* 20 (2018) 10275–10285. <https://doi.org/10.1039/C7CP07939G>.
- [63] C. Zhan, J. Neal, J. Wu, D. Jiang, Quantum Effects on the Capacitance of Graphene-Based Electrodes, *J. Phys. Chem. C.* (2015). <https://doi.org/10.1021/acs.jpcc.5b05930>.
- [64] A.C. Forse, C. Merlet, J.M. Griffin, C.P. Grey, New Perspectives on the Charging Mechanisms of Supercapacitors, *J. Am. Chem. Soc.* 138 (2016) 5731–5744. <https://doi.org/10.1021/jacs.6b02115>.
- [65] C. Cruz, A. Ciach, E. Lomba, S. Kondrat, Electrical Double Layers Close to Ionic Liquid–Solvent Demixing, *J. Phys. Chem. C.* 123 (2019) 1596–1601. <https://doi.org/10.1021/acs.jpcc.8b09772>.
- [66] V. Ivaništšev, S. O’Connor, M.V. Fedorov, Poly(a)morphic portrait of the electrical double layer in ionic liquids, *Electrochem. Commun.* 48 (2014) 61–64. <https://doi.org/10.1016/j.elecom.2014.08.014>.
- [67] K. Karu, E. Roos Nerut, X. Tao, S.A. Kislenko, I.V. Voroshylova, V.B. Ivanistsev, Ion monolayers at electrode–ionic liquid interfaces: maximal density and potential drop, *Unpubl. Results*. (n.d.).
- [68] C. Noh, Y. Jung, Understanding the charging dynamics of an ionic liquid electric double layer capacitor via molecular dynamics simulations, *Phys. Chem. Chem. Phys.* 21 (2019) 6790–6800. <https://doi.org/10.1039/C8CP07200K>.
- [69] S. Xu, S. Xing, S.-S. Pei, V. Ivaništšev, R. Lynden-Bell, S. Baldelli, Molecular Response of 1-Butyl-3-Methylimidazolium Dicyanamide Ionic Liquid at the Graphene Electrode Interface Investigated by Sum Frequency Generation Spectroscopy and Molecular Dynamics Simulations, *J. Phys. Chem. C.* 119 (2015) 26009–26019. <https://doi.org/10.1021/acs.jpcc.5b08736>.
- [70] F. Tang, T. Ohto, T. Hasegawa, M. Bonn, Y. Nagata, $\pi^+-\pi^+$ stacking of imidazolium cations enhances molecular layering of room temperature ionic liquids at their interfaces, *Phys Chem Chem Phys.* 19 (2017) 2850–2856. <https://doi.org/10.1039/C6CP07034E>.
- [71] B. Roling, M. Drüscher, B. Huber, Slow and fast capacitive process taking place at the ionic liquid/electrode interface, *Faraday Discuss.* 154 (2011) 303–311. <https://doi.org/10.1039/C1FD00088H>.
- [72] S.A. Kislenko, Y.O. Moroz, K. Karu, V.B. Ivaništšev, M.V. Fedorov, Calculating the Maximum Density of the Surface Packing of Ions in Ionic Liquids, *Russ. J. Phys. Chem. A.* 92 (2018) 999–1005. <https://doi.org/10.1134/S0036024418050187>.
- [73] D. Boda, D. Henderson, K.Y. Chan, D.T. Wasan, Low temperature anomalies in the properties of the electrochemical interface, *Chem. Phys. Lett.* 308 (1999) 473–478.
- [74] J. Vatamanu, O. Borodin, G.D. Smith, Molecular Insights into the Potential and Temperature Dependences of the Differential Capacitance of a Room-Temperature Ionic Liquid at Graphite Electrodes, *J. Am. Chem. Soc.* 132 (2010) 14825–14833. <https://doi.org/10.1021/ja104273r>.
- [75] S.A. Kislenko, R.H. Amirov, I.S. Samoylov, Molecular dynamics simulation of the electrical double layer in ionic liquids, *J. Phys. Conf. Ser.* 418 (2013) 012021–8. <https://doi.org/10.1088/1742-6596/418/1/012021>.
- [76] K. Ma, J. Forsman, C.E. Woodward, Influence of ion pairing in ionic liquids on electrical double layer structures and surface force using classical density functional approach, *J. Chem. Phys.* 142 (2015) 174704. <https://doi.org/10.1063/1.4919314>.

- [77] J. Xia, F. Chen, J. Li, N. Tao, Measurement of the quantum capacitance of graphene, *Nat. Nanotechnol.* 4 (2009) 505–509. <https://doi.org/10.1038/nnano.2009.177>.
- [78] T. Fang, A. Konar, H. Xing, D. Jena, Carrier statistics and quantum capacitance of graphene sheets and ribbons, *Appl. Phys. Lett.* 91 (2007) 092109. <https://doi.org/10.1063/1.2776887>.
- [79] E. Paek, A.J. Pak, G.S. Hwang, A Computational Study of the Interfacial Structure and Capacitance of Graphene in [BMIM][PF6] Ionic Liquid, *J. Electrochem. Soc.* 160 (2013) A1–A10. <https://doi.org/10.1149/2.019301jes>.
- [80] M. Salanne, Simulations of room temperature ionic liquids: from polarizable to coarse-grained force fields, *Phys. Chem. Chem. Phys.* 17 (2015) 14270–14279. <https://doi.org/10.1039/C4CP05550K>.
- [81] Z. Wang, Y. Yang, D.L. Olmsted, M. Asta, B.B. Laird, Evaluation of the constant potential method in simulating electric double-layer capacitors, *J. Chem. Phys.* 141 (2014) 184102. <https://doi.org/10.1063/1.4899176>.
- [82] K. Goloviznina, J.N. Canongia Lopes, M. Costa Gomes, A.A.H. Pádua, Transferable, Polarizable Force Field for Ionic Liquids, *J. Chem. Theory Comput.* 15 (2019) 5858–5871. <https://doi.org/10.1021/acs.jctc.9b00689>.
- [83] E.A. Vázquez-Montelongo, J.E. Vázquez-Cervantes, G.A. Cisneros, Current Status of AMOEBA-IL: A Multipolar/Polarizable Force Field for Ionic Liquids, *Int. J. Mol. Sci.* 21 (2020) 697. <https://doi.org/10.3390/ijms21030697>.
- [84] C.Y. Son, J.G. McDaniel, J.R. Schmidt, Q. Cui, A. Yethiraj, First-Principles United Atom Force Field for the Ionic Liquid BMIM+BF₄⁻: An Alternative to Charge Scaling, *J. Phys. Chem. B.* 120 (2016) 3560–3568. <https://doi.org/10.1021/acs.jpcc.5b12371>.
- [85] A. Marin-Laflèche, M. Haefele, L. Scalfi, A. Coretti, T. Dufils, G. Jeanmairet, S.K. Reed, S. Alessandra, R. Berthin, C. Bacon, S. Bonella, B. Rotenberg, P.A. Madden, M. Salanne, MetalWalls: A classical molecular dynamics software dedicated to the simulation of electrochemical systems, *J. Open Source Softw.* 5 (2020) 2373. <https://doi.org/10.21105/joss.02373>.
- [86] L. Scalfi, T. Dufils, K.G. Reeves, B. Rotenberg, M. Salanne, A semiclassical Thomas–Fermi model to tune the metallicity of electrodes in molecular simulations, *J. Chem. Phys.* 153 (2020) 174704. <https://doi.org/10.1063/5.0028232>.